Independent population coding of the past and the present in prefrontal cortex during learning

Silvia Maggi[1] and Mark D. Humphries[1*]

1. School of Psychology, University of Nottingham, Nottingham, UK.

* Contact: mark.humphries@nottingham.ac.uk

Abstract

Medial prefrontal cortex (mPfC) plays a role in present behaviour and in short-term memory. Unknown is whether the present and the past are represented in the same mPfC neural population and, if so, how the two representations do not interfere. Analysing mPfC population activity of rats learning rules in a Y-maze, we find population activity switches from encoding the present to encoding the past of the same events after reaching the arm-end. We show the switch is driven by population activity rotating to orthogonal axes, and the population code of the present and not the past reactivates in subsequent sleep, confirming these axes were independently accessible. Our results suggest mPfC solves the interference problem by encoding the past and present on independent axes of activity in the same population, and support a model of the past and present encoding having independent functional roles, respectively contributing to on-line learning and off-line consolidation.

Keywords: decision making, mPFC, learning, neural ensembles, sleep, replay

Introduction

The medial prefrontal cortex (mPfC) plays key roles in adaptive behaviour, including reshaping behaviour in response to changes in a dynamic environment (Euston et al., 2012) and in response to errors in performance (Narayanan and Laubach, 2008; Laubach et al., 2015). Damage to mPfC prevents shifting behavioural strategies when the environment changes (Laskowski et al., 2016; Guise and Shapiro, 2017). Single neurons in mPfC shift the timing of spikes relative to hippocampal theta rhythms just before acquiring a new action-outcome rule (Benchenane et al., 2010). And multiple labs have reported that global shifts in mPfC population activity precede switching between behavioural strategies (Rich and Shapiro, 2009; Durstewitz et al., 2010; Karlsson et al., 2012; Powell and Redish, 2016) and the extinction of learnt associations (Russo et al., 2020).

Adapting behaviour depends on knowledge of both the past and the present. Deep lines of research have established that mPfC activity represents information about both. The memory of the immediate past is maintained in mPfC activity, both in tasks requiring explicit use of working memory (Baeg et al., 2003; Fujisawa et al., 2008; Spellman et al., 2015) and those that do not (Maggi et al., 2018). The use of such memory is seen in both the impairment arising from mPfC lesions (Rich and Shapiro, 2007; Young and Shapiro, 2009; Laskowski et al., 2016), and the role of mPfC in error monitoring (Laubach et al.,

2015). Representations of stimuli and events happening in the present have been reported in a variety of decision-making tasks throughout PfC (Averbeck et al., 2006; Rigotti et al., 2013; Hanks et al., 2015; Siegel et al., 2015), and specifically within rodent mPfC (Sul et al., 2010; Ito et al., 2015; Guise and Shapiro, 2017).

Little is known though about the relationship between representations of the past and present in mPfC activity. Prior studies have shown that past and upcoming choices can both modulate activity of neurons in the same mPfC population (for example Baeg et al., 2003; Ito et al., 2015), but none have compared the encodings of the past and present, nor determined how the encoding of the present becomes the encoding of the past. Thus important questions remain: how the past and present are encoded in the same mPfC population, how the encoding of features in the present transforms into the encoding of the past, and how that transforms solves the problem of potential interference between the past and the present – that the encoding of the past does not overwrite that of the present, or vice-versa, and that the two encodings can be addressed independently.

To address these questions, we reanalyse here mPfC population activity from rats learning new rules on a Y-maze (Peyrache et al., 2009). Crucially, this task had distinct trial and inter-trial interval phases, in which we could respectively examine the population encoding of the present (in trials) and the past (in the intervals) of the same task features or events. We first established that small mPfC populations did indeed encode both the present and past of the same features of the task, respectively in the trial and in the inter-trial interval. We found that these encodings were orthogonal, so that the present and the past were encoded by activity evolving along independent coding axes. Crucially, we show here that these encodings of the past and the present could be addressed independently: population activity encoding the present was reactivated in post-training sleep, but activity encoding the same features in the past was not reactivated. Moreover, the improvement in the animal's performance during a session correlated with how strongly the encoding of the present was reactivated. Thus, by encoding the past and present of the same events on independent axes, a single mPfC population prevents interference between them, and allows their independent recall.

Results

To address how the mPfC encodes the past and the present, we analyse here data from rats learning rules in a Y maze, who had tetrodes implanted in mPfC before the first session of training. Across sessions, animals were asked to learn one of 4 rules, which were given in sequence (go to the right arm, go to the lit arm, go to the left arm, go to the dark arm). Rules were switched after 10 correct choices (or 11 out of 12). There were 8 rule-switch sessions in total, and each animal experienced at least 2 rules. The animal self-initiated each trial by running along the central stem of the Y maze and choosing one of the arms (Figure 1a). The trial finished at the arm's end, and reward delivered if the chosen arm matched the current rule being acquired. During the following inter-trial interval the rat made a self-paced return to the start of the central arm to initiate the next trial. Throughout, population activity was recorded in the prelimbic and infralimbic cortex (Figure 1b), which we shall term medial prefrontal cortex (mPfC) here (Laubach et al., 2018, propose that these regions are equivalent to the anterior cingulate cortex in primates). This task thus allowed us to study the representation of choice and its environmental context in both the present (the trial) and the immediate past (the inter-trial interval).

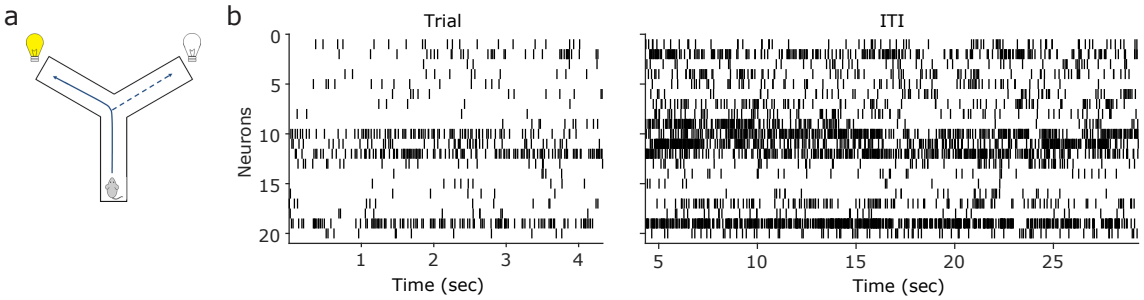

Figure 1: Task and mPfC population activity
(**a**) Schematic of the Y-maze task, showing a rat at the start position. A trial is the period from the start position to the end of the chosen arm; the inter-trial interval is the return from the arm end to the start position. On each trial one arm-end was lit, chosen in a pseudo-random order, irrespective of whether it was relevant to the current enforced rule. Across sessions, animals were asked to learn one of 4 rules in the sequence: go to the right arm, go to the lit arm, go to the left arm, go to the dark arm. Rules switched after 10 correct choices (or 11 out of 12). There were 8 rule-switch sessions in total, and each animal experienced at least 2 rules.
(b) Raster plots of spiking activity in the medial prefrontal cortex during a single trial and the following inter-trial interval (ITI).

Population activity encodes the present and the past of the same task features

In order to compare representations of the same choice and features in the past and present, we first had to establish that these were indeed represented in mPfC population activity. Using a linear decoder on the vector of population activity during each trial or inter-trial interval (Figure 2a), we decoded key features of the task: the animal's choice of arm direction in the trial, the outcome of the trial, and which arm-end was lit during the trial. Population vectors for a given session used neurons active in every trial of that session, so ranged from 4-22 neurons across 49 sessions, of between 7-51 trials each (Figure 2 – SI Figure 1). We trained the same decoders using the same population vectors but with features shuffled across trials (see Methods), to define appropriate chance levels for each decoder given the unbalanced distribution of some task features, such as outcome.

We could decode all of direction choice, outcome, and light position in the current trial above chance (Figure 2b,d, left). In Figure 2b we plot the absolute accuracy of decoding, to show that the decoding could be near-perfect; in Figure 2d we also plot the decoding accuracy relative to the shuffled data for each session, which, as it accounts for the different distributions of features (e.g. outcome) in each session, better shows the effect size of the decoding. To test for effects of task history on population activity, we also decoded the direction choice, outcome, and light position of the preceding trial, and found that decoding was at or close to chance (Figure 2b,d, right).

By contrast, from population activity during the inter-trial interval we could decode the direction choice, outcome, and light position of the immediately preceding trial well above chance (Figure 2c,e, right). Decoding the same feature of the immediately following trial was at chance (Figure 2c,e, left). Thus, the present and the past of key features of a trial could both be decoded from mPfC population activity: the present direction choice, outcome, and light position during the trial, and the past direction choice, outcome, and light position during the inter-trial interval.

We explored the extent to which this decoding of the present in trials and of the past in the inter-trial intervals depended on what occurred during each session. We first split the sessions by whether the target rule was direction-based (15 sessions), and thus egocentric,

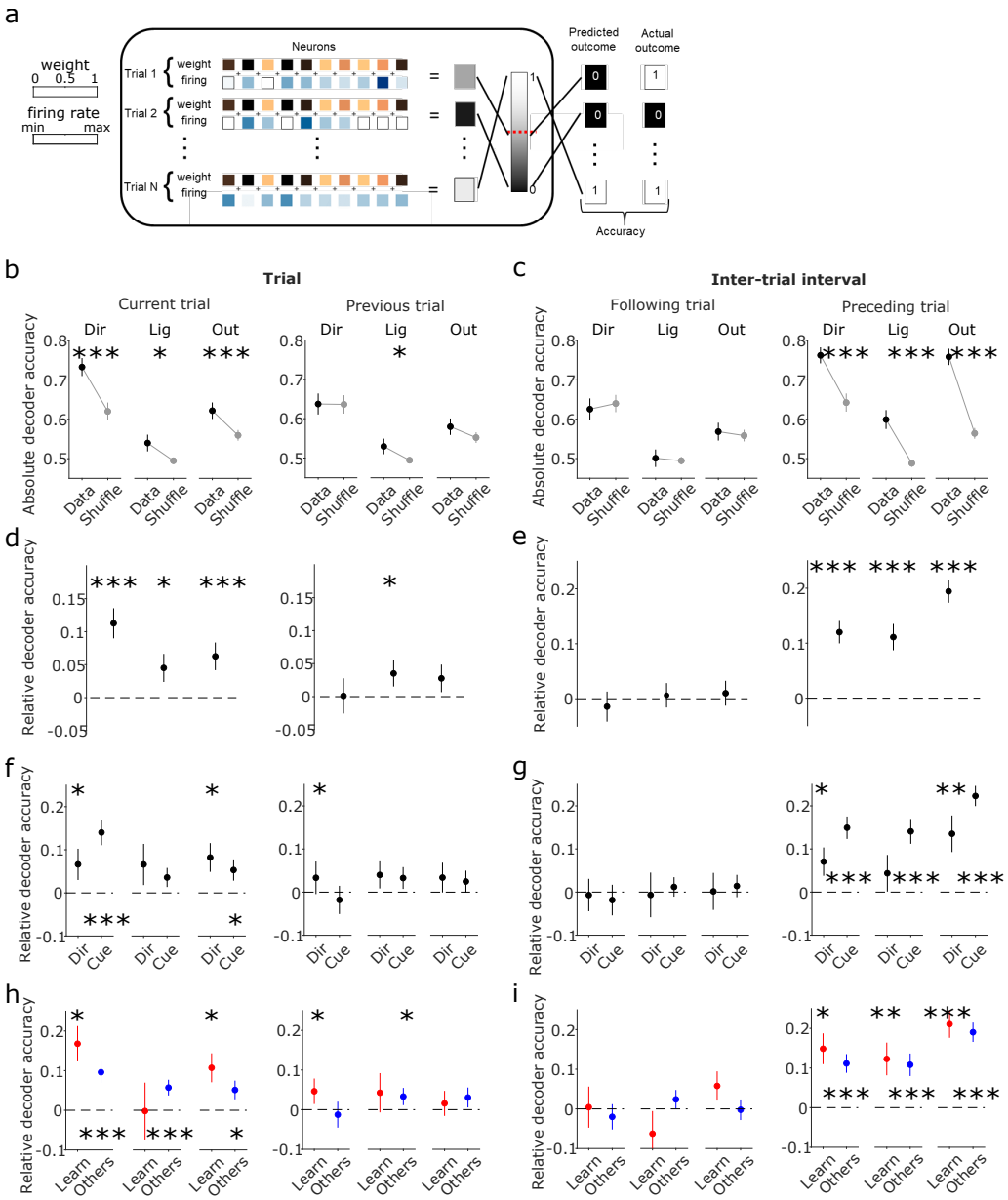

Figure 2: PfC population encoding of the past and present of the same task features
(**a**) Schematic of a linear decoder of population activity during a session's trials. Trials were repeatedly divided into a training set and one held-out test trial. The population vector of neuron firing rates for each trial in the training set (shade of blue squares) is input to a linear decoder that fits the weight (shade of yellow squares) for each neuron across the trials. A linear combination of the learnt weight vector and the firing rate vector of the trials is compared to a threshold (red dashed line) to predict the category to which that trial belongs. Decoding accuracy is the proportion of correctly predicted held-out trials when using the weight vector from their corresponding training set trials.
(**b**) Decoding accuracy for population activity during the trials of each session. In black we plot the accuracy of decoding the choice of arm direction (Dir), light position (Lig), and outcome (Out) for the current trial (left panel), and the previous trial (right panel). In grey we plot the decoding accuracy of shuffled labels across trials. Significant data decoding was tested using paired Wilcoxon signed rank test: * $p < 0.05$; ** $p < 0.01$; *** $p < 0.001$. Symbols plot means ± SEM across 49 sessions.
(**c**) as for panel (b), but for population activity during the inter-trial intervals (ITI) of each session.
(**d**)–(**e**) as for panels (b)-(c), but using each session's relative decoding accuracy: the difference between the decoding accuracy of the data and of the mean of the shuffled data in that session. Here and all further panels, P-values are given for a Wilcoxon signed rank test against zero median.
(**f**) Breakdown of the trial decoding results in panel (d) by the rule type of each session (15 direction rule sessions; 34 cue rule sessions).
(**g**) As for panel (f), breakdown of the inter-trial interval decoding results by the rule-type of each session.
(**h**) Breakdown of the trial decoding results in panel (d) by whether a rule was learnt in a session

or cue-based (34 sessions) and thus allocentric. For trials, the present direction choice and outcome could still be significantly decoded for both types of rule, despite the considerable drop in power from 49 to 15 and 34 sessions (Figure 2f). For inter-trial intervals, the preceding direction choice, outcome, and light position could still be decoded well above chance for both types of rule (Figure 2g).

In order to determine if learning itself affected any mPfC representations of the present, we then separated the sessions into two behavioural groups: putative learning sessions ($n = 10$), identified by a step-change in task performance (Figure 2 – Supplementary Figure 2), and the remaining sessions, called here "Other" ($n = 39$). We found decoding of task features was similar when comparing learning sessions and all Other sessions for both trials (Figure 2h) and inter-trial intervals (Figure 2i). The sole exception, of decoding the current light position during trials of Other sessions but not learning sessions, could be due either to a real effect, or to the low power for decoding from 10 learning sessions.

It is likely that the mPfC encoding of task features is partly dependent on maze position (Ito et al., 2015; Spellman et al., 2015). To further examine the evolution of encoding over the trial and inter-trial interval, we divided the maze into five equally sized sections, and constructed population firing rate vectors for each position (Figure 2 – Supplementary Figure 3). Even though the trials averaged only 4 seconds in duration, and so each position was occupied for one second or less, we still obtained clear evidence for decoding the current trial's direction choice, outcome, and light position across multiple contiguous locations. The contrast between the strong encoding of the current trial's features and the weak encoding of the previous trial's features was even clearer across maze positions. Figure 2–Supplementary Figure 4 confirms that these results are robust to breaking down the position decoding by the type of rule or by learning behaviour. Crucially, no matter how we examined the decoding by position, it showed that the population encoding is contiguous from the trial to the following inter-trial interval for all three features (see esp. Figure 2 – Supplementary Figure 3b): the encoding of the present in the trial at the arm end is immediately transformed into the encoding of the past in the inter-trial interval.

Independent encoding of the past and the present

Having established evidence that a single mPfC population encodes both the present and the past of the same features of a rule-learning task, we could now address the key question of the relationship between these representations. In particular, we sought to address how encoding of features in the present transforms into the encoding of the past, and if this is done in a way to minimise interference between them, such that the representations of the past and present can be independently accessed and activated.

One hypothesis is that there is no transformation: that sustained activity in mPfC continues from the trial into the inter-trial interval, creating a memory trace of the encoding during the trial. Another plausible hypothesis is that the population activity in the trial reactivates during the inter-trial interval, in some form of replay of waking activity. Both hypotheses predict that the population encoding of a feature in the trial and in the following inter-trial interval should be the same. We show here it is not.

One simple way to rule out the memory trace and reactivation hypotheses would be if the active neurons during the trial and inter-trial interval were different. However, the active neurons during the trials were also active during the inter-trial interval (Figure 2 - Supplemental Figure 1c), so this shared common population could, in principle, carry on encoding the same task features.

We used this common population to test whether mPfC populations were encoding the past and the present in the same way: if the encoding was broadly the same, then

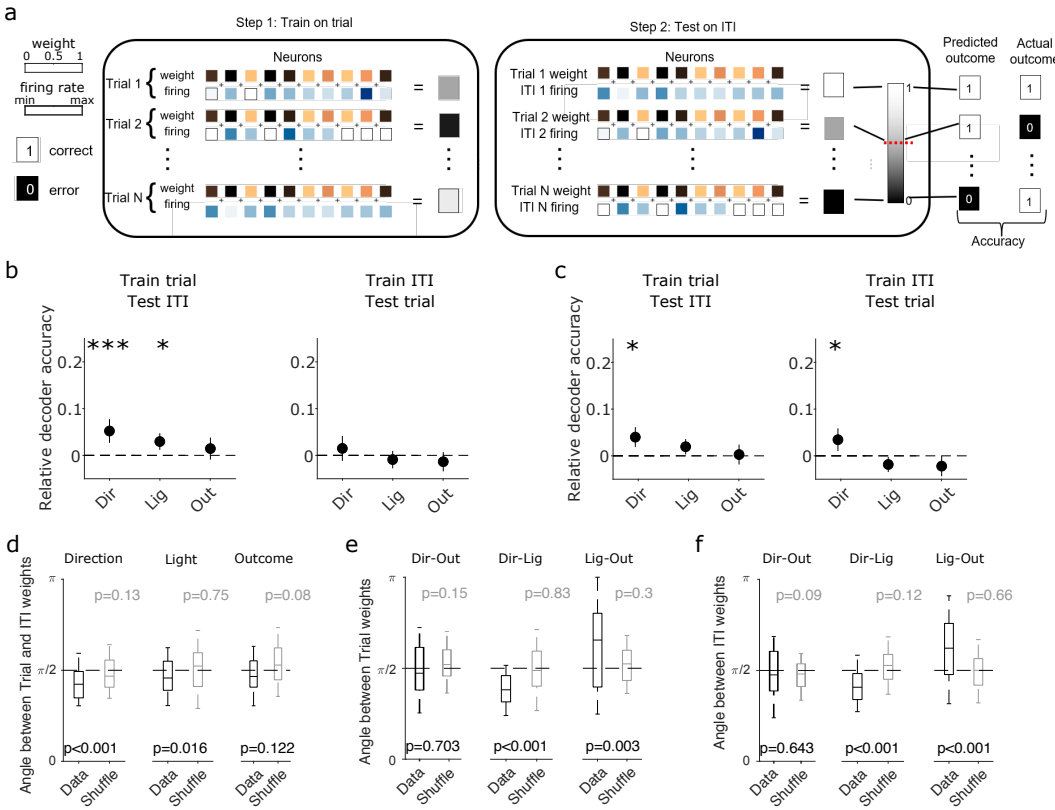

Figure 3: Independent population encoding of past and present task events.
(**a**) Schematic of cross-decoding the same task feature. We train the decoder of a feature using the activity in the trials of a session, then test the accuracy of decoding the same feature (now in the past) from the activity in the inter-trial intervals. (Or vice-versa: training the decoder on the inter-trial intervals (ITIs), and testing the decoding accuracy on the trials). We did this in two ways. First, as per Figure 2, we used leave-one-out cross validation, by leaving out the ith trial-ITI pair, training on $N-1$ trials, and predicting the ith ITI. Second we used full cross-decoding, training the decoder on all N trials to get one weight vector for the decoder, and testing the decoding accuracy on all ITIs using that vector (and vice-versa).
(**b**) Cross-decoding performance for each task feature of the current trial, using leave-one-out cross-validation. Left: performance when the decoder was trained on activity during trials and tested on activity in the inter-trial intervals. Black dashed line shows the chance levels obtained training the classifier on shuffled labels for the trials and testing on inter-trial intervals given the same shuffled labels. Right: performance when the decoder was trained on activity from the inter-trial intervals, and tested on activity in the trials.
(**c**) As per (b), cross-decoding performance of the same task feature, using full cross-decoding.
(**d**) Comparison of the decoding vector weights between trials and inter-trial intervals. For each session we plot the angle between its trial and inter-trial interval decoding weight vectors, obtained from the trained decoders in panel (c). For reference, we also compute the angle between trial and inter-trial interval decoding vectors obtained by training on shuffled label data (grey). Boxplots show median (line), inter-quartile range (box), and 95% interval (tails). P-values are from Wilcoxon ranksum tests for the difference from $\pi/2$.
(**e**) As for (d), but comparing the decoding weight vectors between features, within trials.
(**f**) As for (e), for within inter-trial intervals.

the activity in the trial and following inter-trial interval should be interchangeable when predicting the same feature, such as the chosen direction. In this cross-decoding test (Figure 3a), we first trained a linear decoder for features of the present using the common

population's activity during the trials, and then tested the accuracy of the linear decoder when using the common population's activity during the inter-trial interval. If the population encoding in the trials was re-used in the inter-trial interval, then this cross-decoding should be accurate.

We found that cross-decoding of features was consistently poor, whether we trained on trial activity and tested on inter-trial intervals, or vice-versa (Figure 3b). Decoding of all features was at or close to chance, strikingly at odds with the within-trial (Figure 2b,d) or within-interval (Figure 2c,e) decoding. This poor cross-decoding was robust to whether we used leave-one-out cross-validation (Figure 3b), or trained the decoder on every trial or every inter-trial interval (Figure 3c). We also found consistently poor cross-decoding of all features when we tested at different positions along the maze (Figure 3 – Supplemental Figure 1). These results suggest that population encoding of prior events in the inter-trial interval is not simply a memory trace or reactivation of similar activity in the trial. Instead, they show that the same mPfC population is separately and independently encoding the present and past of the same features.

To quantify this independence, we turned to the vector of decoding weights for the trials and the equivalent vector for the inter-trial intervals of the same session. These weights, obtained from the decoder trained once on all trials and then once on all inter-trial intervals, give the relative contribution of each neuron to the encoding of task features. We found that the trial and inter-trial interval weight vectors were approximately orthogonal for all three features: the angles cluster at or close to $\pi/2$ (or, equivalently, their dot-product clusters at or around zero) (Fig 3d). Median angles for direction choice and light position were significantly less than $\pi/2$ (ranksum test), but the difference was small: 0.067π for direction and 0.045π for light position. Thus, the population encoding in the inter-trial interval was not a memory trace: to a good approximation, the past and present are orthogonally encoded in the same mPfC population.

We considered a range of alternative explanations for these results. One is that the orthogonality arises from the curse of dimensionality: the distance between two i.i.d random vectors with a mean of zero tends to grow with their increasing dimension. If the decoding weights were random vectors, then the apparent orthogonality could be driven by just the largest mPfC populations. However, the decoding weights for the whole trial (present) or whole inter-trial interval (past) are not random vectors, for if they were then decoding performance would be at chance, whereas we find clear decoding of all features (Figure 2b-e). Another explanation is that the independent encoding axes between the trials and inter-trial intervals is somehow driven by differing properties of the trials and inter-trial intervals. For example, they differ in duration (mean 6.5 $\pm$ 0.01 seconds for trials, 55.7 $\pm$ 0.03 seconds for inter-trial intervals), and hence also in average movement speed. If switching between trials and inter-trial intervals could account for encoding differences, then these differences should be symmetric: we should see encodings change whether the transition was from the trial to inter-trial interval, or from the inter-trial interval back to a trial. However, the encodings were asymmetric: we saw strong encoding during the transition from trial to inter-trial interval (Figure 2b-c and Figure 2 – Supplementary Figure 3), but no encoding during the transition from inter-trial interval back to the trial (Figure 2b-c and Figure 2 – Supplementary Figure 3; and see Maggi et al. (2018)). In the absence of any encoding, there cannot be an orthogonal shift in encoding.

To understand how the independent encoding between past and present related to how the features were jointly encoded in the population activity, we examined the relationship between the features' encoding vectors during the trial and during the inter-trial interval. The encoding axes within an epoch were less independent than between epochs: angles

between the encoding vectors for light and direction and for light and outcome were significantly different from $\pi/2$ (Figure 3e,f). But the distributions of angles between the encoding vectors were preserved between the trials and the inter-trial intervals, with outcome-direction around $\pi/2$, light-direction centered below $\pi/2$, and light-outcome centred above $\pi/2$. Thus, while each encoding axis rotated to an orthogonal direction between the trial and inter-trial interval, the internal relationships between the feature encodings was preserved.

Population activity rotates between trials and inter-trial intervals

That all three feature encodings were independent between the trials and inter-trial intervals of a session predicts that the population activity itself should be independent between the two. If true, then trial and inter-trial interval population activity vectors should be easily separable. To test this prediction, we projected all population activity vectors of a session (Fig 4a) into a low dimensional space (Fig 4b), and then quantified how easily we could separate them into trials and inter-trial intervals. Using just one dimension was sufficient for near-perfect separation in many sessions; using two was sufficient for above-chance performance in all sessions (Fig 4c; and see Figure 4 – Supplementary Figure 1 for a breakdown of each session's dependence on the number dimensions). Population activity was thus about as independent between the trials and inter-trial intervals as it possibly could be.

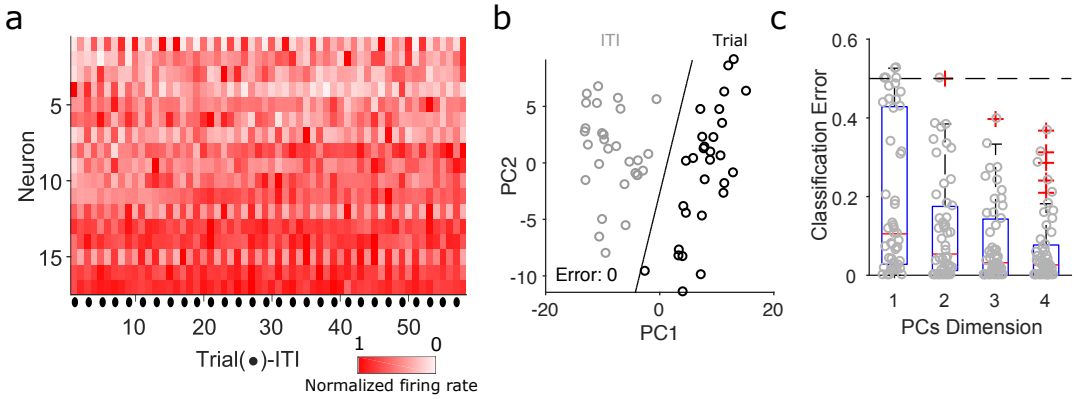

Figure 4: Population activity is independent between trials and inter-trial intervals
(**a**) Population activity vectors for the trials (•) and following inter-trial intervals of one session. The heat-map shows the normalized firing rate for each neuron.
(**b**) Projection of that session's population activity vectors on to two dimensions shows a complete separation of trial and inter-trial interval activity. The black line is the linear separation found by the classifier. PC: principal component.
(**c**) Summary of classification error over all sessions, as a function of the number of dimensions. Each grey dot is the error for one session at that number of projecting dimensions. Dashed line gives chance performance. Boxplots show medians (red line), interquartile ranges (blue box), and outliers (red pluses).

The independence in the population activity might arise from the continuous evolution of mPfC population activity across the contiguous trial and inter-trial interval period, such as the sequential activation of PfC neurons observed in previous studies (e.g. Fujisawa et al., 2008). If sequential activation was ongoing, then we should also observe consistently independent population activity between consecutive sections of the maze during trials and during inter-trial intervals. Instead, we found population activity was not independent between contiguous maze sections within trials or within inter-trial intervals (Figure 4 –

Supplementary Figure 2a-c). Across the whole maze, population vectors from adjacent sections within trials and inter-trial intervals had classification errors consistently greater than any found between trials and inter-trial intervals (Figure 4 – Supplementary Figure 2), even when the animal was in the same maze position. Thus, while population activity evolved during the trial and during the inter-trial interval, corresponding to the evolution of feature encoding across the maze (Figure 2 – Supplementary Figure 3), this evolution happened along independent directions in the trials and in the inter-trial intervals.

Population representations of trial features re-activate in sleep

Encoding the past and present of the same features in the same population faces the problem of interference: of how a downstream read-out of the population's activity knows whether it is reading out the past or the present. Our finding that the encoding is on independent axes means that, in principle, the representations of past and present can be addressed or recalled independently, without interfering with each other. We thus sought further evidence of this independent encoding by asking if either representation could be recalled independently of the other.

Prior reports showed that patterns of mPfC population activity during training are preferentially repeated in post-training slow-wave sleep (Euston et al., 2007; Peyrache et al., 2009; Singh et al., 2019), consistent with a role in memory consolidation. However, it is unknown what features these repeated patterns encode, and whether they encode the past or the present or both. Thus, we took advantage of the fact that our mPfC populations were also recorded during both pre- and post-training sleep to ask which, if any, of the trial and inter-trial interval codes are reactivated in sleep, and thus whether they were recalled independently of each other.

We first tested whether population activity representations in trials reactivated more in post-training than pre-training sleep. For each feature of the task happening in the present (e.g choosing the left arm), we followed the decoding results by creating a population vector of the activity specific to that feature during a session's trials. To seek their appearance in slow-wave sleep, we computed population firing rate vectors in pre- and post-training slow-wave sleep in time bins of 1 second duration, and correlated each sleep vector with the feature-specific trial vector (Figure 5a). We thus obtained a distribution of correlations between the trial-vector and all pre-training sleep vectors, and a similar distribution between the trial-vector and all post-training sleep vectors. Greater correlation with post-training sleep activity would then be evidence of preferential reactivation of feature-specific activity in post-training sleep.

We examined reactivation separately between learning and Other sessions, seeking consistency with previous reports that reactivation of waking population activity in mPfC most clearly occurs immediately after rule acquisition (Peyrache et al., 2009; Singh et al., 2019). Figure 5b (upper panels) shows a clear example of a learning session with preferential reactivation. For all trial features, the distribution of correlations between the trial and post-training sleep population activity is right-shifted from the distribution for pre-training sleep. For example, the population activity vector for choosing the right arm is more correlated with activity vectors in post-training (Post-R) than pre-training (Pre-R) sleep.

Such post-training reactivation was not inevitable. In Figure 5b (lower panels), we plot another example in which the trial-activity vector equally correlates with population activity in pre- and post-training sleep. Even though specific pairs of features (such as the left and right light positions) differed in their overall correlation between sleep and trial activity, no feature shows preferential reactivation in post-training sleep.

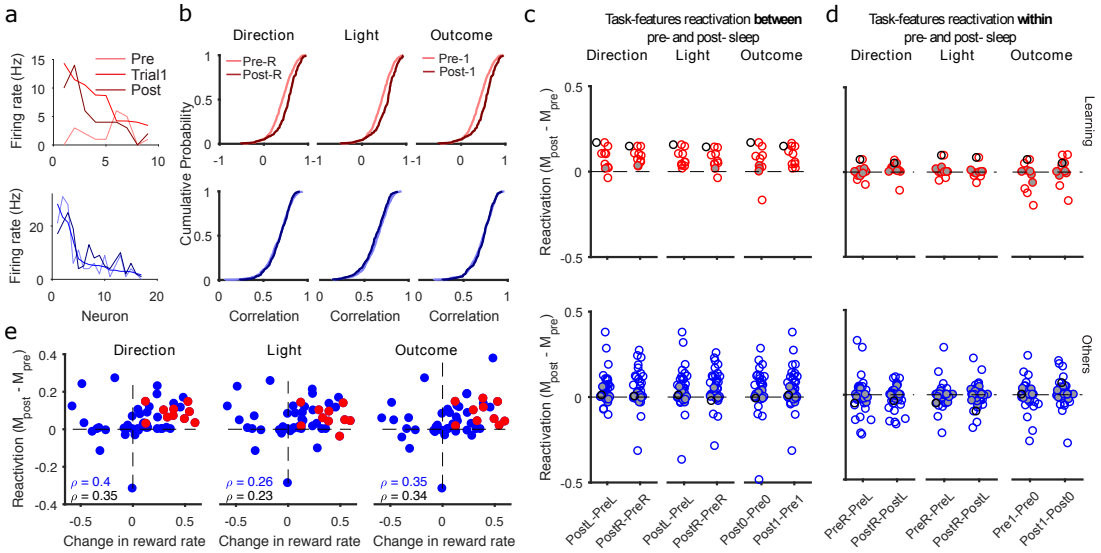

Figure 5: Reactivation of trial population coding in post-training sleep.
(**a**) Example population activity vectors. Upper panel: from one learning session, we plot the average firing rate vector for correct trials (Trial1). For comparison, we also plot examples of firing rate vectors from pre- and post-training slow-wave sleep (1s bins). Neurons are ranked in order of their firing rates in the trial vector. Lower panel: as for the upper panel, for an example session not classified as learning.
(**b**) Example distributions of Spearman's rank correlations between trial and sleep population activity. Upper panels: for the same learning session as panel (a), we plot the distributions of correlations between each vector of feature-specific trial activity and the population activity vectors in pre- and post-training slow-wave sleep. Lower panels: as for the upper panels, for the example non-learning session in panel (a). R: right arm; 1: rewarded trial.
(**c**) Summary of reactivations across all sessions. For each feature, we plot the difference between the medians of the pre- and post-training correlation distributions. A difference greater than zero indicates greater correlation between trials and post-training sleep. Each symbol is a session. Empty symbols are sessions with significantly different correlation distributions at $p < 0.05$ (Kolmogorov-Smirnov test). Grey filled symbols are not significantly different. One black circle for learning and one for non-learning sessions identify the two example sessions in panels (a) and (b).
(**d**) As for panel c, but plotting the median differences between distributions for paired features within the same sleep epoch. For example, in the left-most column, we plot the difference between the correlations with pre-session sleep activity for right-choice and left-choice specific trial vectors (PreR - PreL).
(**e**) Reactivation as a function of the change in reward rate in a session. One symbol per session: learning (red); Other (blue). ρ: Spearman's correlation coefficient. Black ρ is for all 49 sessions; blue ρ, using only sessions with any incremental improvement in performance ($N = 33$ in total, 10 learning and 23 Other sessions; see Methods). We plot here reactivation of vectors corresponding to left (direction and light) or correct; correlations for other vectors are similar in magnitude: 0.37 (choose right), 0.35 (cue on right), 0.2 (error trials) for all 49 sessions; 0.37 (choose left), 0.33 (cue on right) and 0.26 (error trials) for sessions with incremental improvement in performance.

These examples were recapitulated across the data (Figure 5c). In learning sessions, feature-specific activity vectors were consistently more correlated with activity in post- than pre-training sleep. By contrast, the Other sessions showed no consistent preferential reactivation of any feature vector in post-training sleep. As a control for statistical artefacts in our reactivation analysis, we looked for differences in reactivation between paired

features (e.g. left versus right arm choice) within the same sleep epoch and found these all centre on zero (Figure 5d). Thus, population representations of task features in the present were reactivated in sleep, and this consistently occurred after a learning session.

To check whether reactivation was unique to step-like learning, we turned to the Other sessions: there we found a wide distribution of preferential reactivation, from many about zero to a few reactivated nearly as strongly as in the learning sessions (Figure 5c, blue symbols). Indeed, when pooled with the learning sessions, we found reactivation of a feature vector in post-training sleep was correlated with the increase in accumulated reward during the session's trials (Fig 5e). Consequently, reactivation of population encoding during sleep may be directly linked to the preceding improvement in performance.

Prior reports suggest that the reactivation of activity patterns in sleep can be faster or slower during sleep than they were during waking activity. We tested the time-scale dependence of feature-vector reactivation by varying the size of the bins used to create population vectors in sleep, with larger bins corresponding to slower reactivation. We found that preferential reactivation in post-training sleep in learning and (some) Other sessions was robust over orders of magnitude of vector widths (Figure 6a). Notably, in the learning sessions only the vectors for rewarded outcome were significantly reactivated. Moreover, among Other sessions, the reactivation in post-training sleep was significant only for those sessions in which the animal's performance improved (however slightly) within the session (Figure 6b). This consistency across broad time-scales suggests that it is the changes during trials to the relative excitability of neurons within the mPfC population that are carried forward into sleep (Singh et al., 2019). Thus, this consistency across broad time-scales implies that whenever the encoding neurons are active, they are active together with approximately the same ordering of firing rates.

No re-activation in sleep of inter-trial interval feature representations

To ask if this reactivation was unique to encoding of the present, we repeated the same reactivation analysis for population vectors from the inter-trial interval. Again, following our decoding results, each population feature vector was created from the average activity during inter-trial intervals after that feature (e.g. choose left) had occurred. We then checked for reactivation of this feature vector in pre- and post-training slow-wave sleep.

We found absent or weak preferential reactivation of population encoding in post-training sleep, for any feature in any type of session (Figure 7a). Consistent with this, we found no correlation between the change in performance during a session and the reactivation of feature vectors after a session (Figure 7b). The orthogonal population encoding during sessions (Figure 3) thus appears functional: population encoding of features in the present was reactivated in sleep, but encoding of the same features in the past was not.

Discussion

We have shown that medial PfC population activity independently represents the past and present of the same task features. First, we showed that the same task feature, such as the choice of arm, is encoded by the same population in both the trials and the inter-trial intervals, as respectively the present and past of that feature. Second, vectors of population activity were about as independent between the trials and following inter-trial intervals as they could possibly be. Consequently, within mPfC populations, the past and the present of each feature were encoded on independent axes. Finally, we showed that these independent axes indeed allow the past and present encodings to be independently

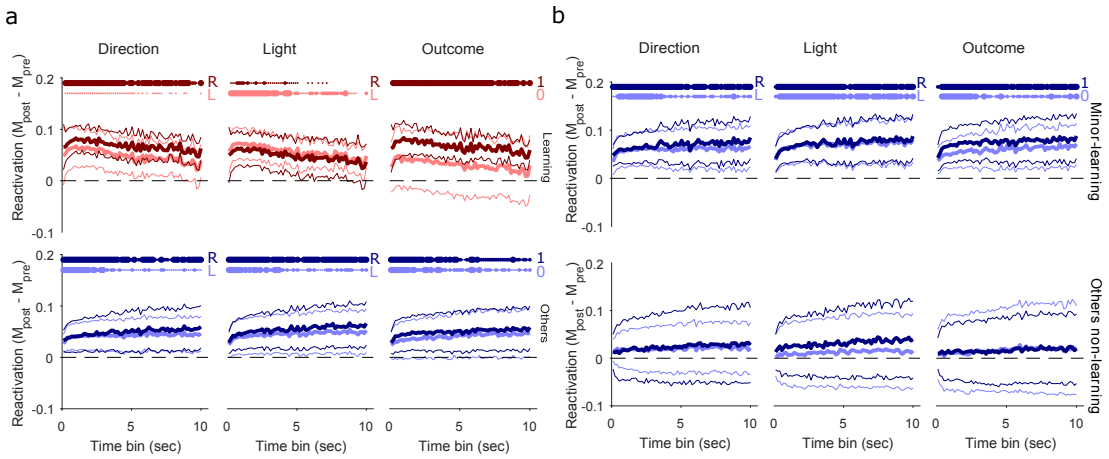

Figure 6: Robust reactivation of trial population coding across time-scales of sleep activity.
(**a**) At each time bin used to construct population activity vectors in sleep, we plot the distribution over sessions of the median differences between pre- and post-training correlation distributions, for learning (top), and other (bottom) sessions. Distributions are plotted as the mean (thick lines) ± 2 SEM (thin lines); at the 1s bin, these summarise the distributions shown in full in Figure 5c. Each panel plots two distributions, one per pair of features: lighter colours indicate left or error trials (L or 0); while darker colours indicate right or correct trials (R or 1). Time bins range from 100 ms to 10 s, tested every 150 ms. Dotted lines at the top of each panel indicate bins with reactivation significantly above zero (Wilcoxon sign rank test, $p < 0.05$ thin dot; $p < 0.01$ middle size dot; $p < 0.005$ thicker dots; $N = 10$ learning, $N = 39$ Other sessions).
(**b**) Here we divide the Other sessions from panel (a) into those showing any increment in performance from the animal ($N = 23$, "Minor-learning", see Methods) and those that did not ($N = 16$).

addressed: population activity representations of features during the trials are re-activated in post-training sleep, but inter-trial interval representations are not.

Mixed population coding in mPfC

Consistent with prior reports of mixed or multiplexed coding by single neurons in the prefrontal cortex (Jung et al., 1998; Horst and Laubach, 2012; Rigotti et al., 2013; Fusi et al., 2016; Aoi et al., 2020), we found that small mPfC populations can sustain mixed encoding of two or more of the current trial's direction choice, light position, and outcome. These encodings were also position-dependent. Encoding of direction choice reliably occurred from the maze's choice point onwards, but it is unclear whether this represents a causal role in the choice itself, or an ongoing representation of a choice being made.

Previous studies have reported encoding of past choices in mPfC population activity during trials (Baeg et al., 2003; Sul et al., 2010). In contrast to the robust encoding of the present, we found weak evidence that mPfC activity during a trial encoded the light position of the previous trial, and weak evidence that it encoded the previous trial's direction choice only during direction-based rules (and note that knowledge of the previous trial's choice was not required for the direction rules). Moreover, we showed these could only be decoded at one or two locations on the maze. Thus, during trials population activity in the prefrontal cortex had robust, sustained encoding of multiple events of the present, but at best weakly and transiently encoded one event of the past.

We also report that these mixed encodings of the present within each population reactivate in post-training sleep. This finding goes beyond prior reports that specific

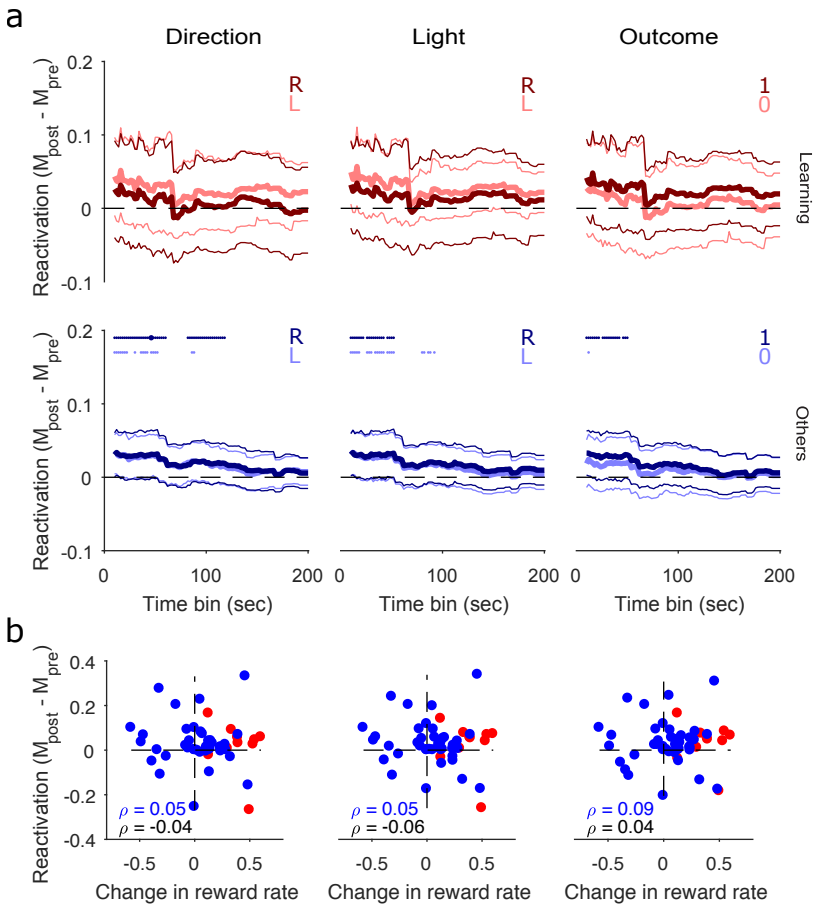

Figure 7: No consistent reactivation of population encoding of the past.
(**a**) Similar to Figure 6, for reactivation of population feature-vectors constructed from inter-trial interval activity. We plot the distribution over sessions of the median differences between pre- and post-training correlation distributions, for learning (top), and Other (bottom) sessions. Note that the range of sleep vector time-bins is an order of magnitude larger than for trials, as the inter-trial intervals themselves are an order of magnitude longer than trials. Dotted lines at the top indicate significant reactivation (Wilcoxon sign rank test, $p < 0.05$ thin dot; $p < 0.01$ middle size dot; $p < 0.005$ thicker dots). Lighter colours indicate left or error trials (L or 0); while darker colours indicate right or correct trials (R or 1)
(**b**) Similar to Figure 5e, reactivation of the inter-trial interval population vector as a function of the change in reward rate in a session. Reactivation is computed for 22 s bins. One symbol per session: learning (red); Other (blue). ρ: Spearman's correlation coefficient; black, all sessions; blue, only sessions with any incremental improvement in performance. We plot here reactivation of vectors corresponding to left (direction and light) or correct trials; correlations for other vectors are similar in magnitude: -0.004 (choose right), 0.02 (cue on right), -0.08 (error trials) for all sessions; -0.005 (choose right), 0.01 (cue on right) and -0.1 (error trials) for sessions with incremental improvement in performance.

patterns of trial activity reactivate in sleep (Euston et al., 2007; Peyrache et al., 2009; Singh et al., 2019) to show what those patterns were encoding – multiple features of the present, but not the past. It seems mixed encoding is a feature of sleep too.

As we showed in (Maggi et al., 2018) and extended here, population activity during the inter-trial interval also has mixed encoding of features of the past. Collectively, our results show that population activity in mPfC can switch from mixed encoding of the present in a trial to mixed encoding of the past in the following inter-trial interval.

Independent population codes solve interference of past and present

There are multiple hypotheses for how this transition from coding the present to the past could happen. One hypothesis is that there are groups of neurons separately dedicated to encoding the past and present. We ruled out this idea by only decoding from neurons active in every trial and inter-trial interval, so showing that the transition from present to past happened within the same group.

Another hypothesis, as we noted in the Results, is that the switching from a population encoding of the present to encoding of the past is explained by population activity in the trials being carried forward into the inter-trial interval, whether by persistent activity acting as a memory trace, or by the recall of patterns of trial activity during the inter-trial interval. But our demonstration of independent encoding in the population between trials and the following inter-trial intervals rules out this hypothesis.

Our results support dynamic coding in mPfC: population encoding evolved within both the trials and the inter-trial intervals, consistent with the underlying changes we observed in the population activity. The evolution of population dynamics over the inter-trial interval is consistent with reports of dynamic changes of PfC activity during the delay period of working memory tasks in primates (Murray et al., 2017; Spaak et al., 2017; Wasmuht et al., 2018), including in primate anterior cingulate cortex (Cavanagh et al., 2018), a potential homologue of the medial prefrontal cortex in rodents (Laubach et al., 2018). The evolving coding we observed thus supports the hypothesis that working memory is sustained by population activity rather than the persistent activity of single neurons (Constantinidis et al., 2018; Lundqvist et al., 2018). Crucially, the evolution of activity within trials and inter-trial intervals was continuous, with adjacent maze sections containing more similar population activity, yet the transition from the trial to the inter-trial interval was discontinuous, with population activity moving to an independent axis. Our results thus show that the evolution of encoding of the present and of the past was each along two independent axes.

Any neural population encoding both the past and the present in its activity faces problems of interference: of how to prevent the addition of new information in the present from overwriting the encoded information of the short-term past (Libby and Buschman, 2019); of how inputs to the population can selectively recall only the past or the present, but not both; and of how downstream populations can access or distinguish the encodings of the past and the present. Representing the present and past on independent axes solves these problems. It means that the encoding of the present can be updated without altering the encoding of the past, that inputs to the population can activate either the past or the present representations independently, and that downstream populations can distinguish the two by being tuned to read-out from one axis or the other. Indeed, we showed that in post-session sleep the encoding of the present can be accessed independently of the encoding of the past.

An open question is how much the clean independence between the encoding of the past and present depends on the behavioural task. In the Y-maze task design, there is a qualitative distinction between trials (with a forced choice) and inter-trial intervals (with a self-paced return to the start arm), which we used to clearly distinguish encoding of the present and the past. Such independent coding may be harder to uncover in tasks without a distinct separation of decision and non-decision phases. For example, tasks where the future choice of arm depends on recent history, such as double-ended T-mazes (Jones and Wilson, 2005), multi-arm sequence mazes (Poucet et al., 1991), or delayed non-match to place (Spellman et al., 2015), blur the separation of the present and the past. Comparing population-level decoding of the past and present in such tasks would give useful insights

into when the two are, and are not, independently coded.

Mechanisms for rapid switching of population codes

The independent encoding and independent population activity between the trial and immediately following inter-trial interval implies a rapid rotation of population activity. How might such a rapid switch of network-wide activity be achieved?

Such rapid switching in the state of a network suggests a switch in the driver inputs to the network. In this model, drive from one source input creates the network states for population encoding A; a change of drive – from another source, or a qualitative change from the same source -— creates the network states for population encoding B (either set of states may of course arise solely from internal dynamics). One option for a switching drive is the hippocampal-prefrontal pathway.

Learning correlates with increased cortico-hippocampal coherence at the choice point of this Y maze (Benchenane et al., 2010; Peyrache et al., 2009). This coherence recurred during slow-wave ripples in post-training sleep. These data and our analyses here are consistent with the population encoding of the trials being (partly) driven by hippocampal input, and with the re-activation of only the trial representations in sleep being the recruitment of those states by hippocampal input during slow-wave sleep. The increased coherence between hippocampus and mPfC activity may act as a window for synaptic plasticity of that pathway (Benchenane et al., 2010, 2011). Consistent with this, we saw a correlation between performance improvement in trials and reactivation in sleep (see also Maingret et al., 2016).

All of which suggests the encoding of the past during the inter-trial interval is not driven by the hippocampal input to mPfC, as its representation is not re-activated in sleep. (Spellman et al. 2015 report hippocampal input to mPfC is necessary for the maintenance of a cue location; though, unlike in our task, actively maintaining the location of this cue was necessary for a later direction decision). Rather, the population coding during the inter-trial interval could reflect the internal dynamics of the mPfC circuit. Indeed, network models of working memory in the prefrontal cortex focus on attractor states created by its local network (Compte et al., 2000; Durstewitz et al., 2000; Miller et al., 2005; Wimmer et al., 2014). If somewhere close to the truth, this account of rapid switching suggests that the hippocampal input to mPfC drives population activity in the trial, and a change or reduction in that input allows the mPfC local circuits to create a different internal state during the inter-trial interval. A prediction of this account is that perturbation of the hippocampal input to the mPfC could disrupt its encoding of the past and present in different ways.

Reconciling mPfC roles in memory and choice

We propose that our combined results here and previously (Maggi et al., 2018) support a dual-function model of mPfC population coding, where the independent coding of the past and present respectively support on-line learning and consolidation. This model is somewhat counter-intuitive: our data suggest the representation of the present in mPfC is used for offline learning, whereas the representation of the past is used online to guide behaviour.

Under this model, the role of memory encoding in the inter-trial interval is to guide learning online: reward tags past features whose conjunction led to successful outcomes (for example, the conjunction of turning left when the light is on in the left arm). While

population activity in the inter-trial interval reliably encodes features of the past throughout training, we previously showed that synchrony of the population only consistently occurs immediately before learning (Maggi et al., 2018). This suggests that the synchronisation of mPfC representations of features predicting success is correlated with successful rule-learning. Consistent with such past-encoding contributing to online learning, we show here that the encoding in the inter-trial interval are not carried forward long-term into sleep.

By contrast, we report here representations of the present in the trial are carried forward and reactivated in sleep. Reactivation of waking activity during slow-wave sleep has been repeatedly linked to the consolidation of memories (Stickgold, 2005; Tononi and Cirelli, 2014; Sawangjit et al., 2018). Indeed, interrupting the re-activation of putative waking activity in hippocampus impairs task learning (Girardeau et al., 2009). Thus, under the dual-function model, we propose the reactivation in mPfC of mixed encodings of the present may be consolidating the conjunction of present features and choice that is going to be successful when re-used in future.

Further insight into these and other ideas here would come from stable recordings of the same population across multiple sessions, to track how encoding of the past and present evolves and is or is not reused. In particular, it would be insightful to establish if re-activated trial representations in sleep reappear in subsequent sessions.

Acknowledgments

We thank Adrien Peyrache for the data, discussions, and comments on early drafts of this manuscript, Hazem Toutounji and Martin O'Neill for comments on drafts, and the Humphries' lab past and present (Abhinav Singh, Javier Caballero, Mat Evans, Francois Cinotti, Tomas Fiers) for discussion. This work was supported by the Medical Research Council [grant numbers MR/J008648/1 and MR/P005659/1]. The original data collection was supported by the EU Framework (FP6) "ICEA" grant.

Author Contributions

M.D.H and S.M. designed the analyses. S.M. analysed the data. M.D.H and S.M. wrote the manuscript.

Declaration of Interest

The authors declare no conflicts of interest.

References

Aoi, M. C., Mante, V., and Pillow, J. W. (2020). Prefrontal cortex exhibits multidimensional dynamic encoding during decision-making. *Nature neuroscience*, 23:1410–1420.

Averbeck, B. B., Sohn, J.-W., and Lee, D. (2006). Activity in prefrontal cortex during dynamic selection of action sequences. *Nat Neurosci*, 9:276–282.

Baeg, E. H., Kim, Y. B., Huh, K., Mook-Jung, I., Kim, H. T., and Jung, M. W. (2003). Dynamics of population code for working memory in the prefrontal cortex. *Neuron*, 40(1):177–188.

494 Benchenane, K., Peyrache, A., Khamassi, M., Tierney, P. L., Gioanni, Y., Battaglia, F. P.,
495 and Wiener, S. I. (2010). Coherent theta oscillations and reorganization of spike timing
496 in the hippocampal- prefrontal network upon learning. *Neuron*, 66(6):921–936.

497 Benchenane, K., Tiesinga, P. H., and Battaglia, F. P. (2011). Oscillations in the prefrontal
498 cortex: a gateway to memory and attention. *Curr Opin Neurobiol*, 21(3):475–485.

499 Cavanagh, S. E., Towers, J. P., Wallis, J. D., Hunt, L. T., and Kennerley, S. W. (2018).
500 Reconciling persistent and dynamic hypotheses of working memory coding in prefrontal
501 cortex. *Nature communications*, 9:3498.

502 Compte, A., Brunel, N., Goldman-Rakic, P. S., and Wang, X. J. (2000). Synaptic mecha-
503 nisms and network dynamics underlying spatial working memory in a cortical network
504 model. *Cereb Cortex*, 10:910–923.

505 Constantinidis, C., Funahashi, S., Lee, D., Murray, J. D., Qi, X.-L., Wang, M., and
506 Arnsten, A. F. T. (2018). Persistent spiking activity underlies working memory. *Journal*
507 *of neuroscience*, 38:7020–7028.

508 Durstewitz, D., Seamans, J. K., and Sejnowski, T. J. (2000). Neurocomputational models
509 of working memory. *Nature Neurosience*, 3:1184–1191.

510 Durstewitz, D., Vittoz, N. M., Floresco, S. B., and Seamans, J. K. (2010). Abrupt transi-
511 tions between prefrontal neural ensemble states accompany behavioral transitions during
512 rule learning. *Neuron*, 66(3):438–448.

513 Euston, D. R., Gruber, A. J., and McNaughton, B. L. (2012). The role of medial prefrontal
514 cortex in memory and decision making. *Neuron*, 76(6):1057–1070.

515 Euston, D. R., Tatsuno, M., and McNaughton, B. L. (2007). Fast-forward playback of
516 recent memory sequences in prefrontal cortex during sleep. *Science*, 318(5853):1147–
517 1150.

518 Fujisawa, S., Amarasingham, A., Harrison, M. T., and Buzsaki, G. (2008). Behavior-
519 dependent short-term assembly dynamics in the medial prefrontal cortex. *Nat Neurosci*,
520 11(7):823–833.

521 Fusi, S., Miller, E. K., and Rigotti, M. (2016). Why neurons mix: high dimensionality for
522 higher cognition. *Curr Opin Neurobiol*, 37:66–74.

523 Girardeau, G., Benchenane, K., Wiener, S. I., Buzsáki, G., and Zugaro, M. B. (2009).
524 Selective suppression of hippocampal ripples impairs spatial memory. *Nature Neuro-*
525 *science*, 12:1222–1223.

526 Guise, K. G. and Shapiro, M. L. (2017). Medial prefrontal cortex reduces memory inter-
527 ference by modifying hippocampal encoding. *Neuron*, 94:183–192.e8.

528 Hanks, T. D., Kopec, C. D., Brunton, B. W., Duan, C. A., Erlich, J. C., and Brody, C. D.
529 (2015). Distinct relationships of parietal and prefrontal cortices to evidence accumula-
530 tion. *Nature*, 520:220–223.

531 Hastie, T., Tibshirani, R., and Friedman, J. (2009). *The Elements of Statistical Learning*.
532 Springer, Berlin.

Horst, N. K. and Laubach, M. (2012). Working with memory: evidence for a role for the medial prefrontal cortex in performance monitoring during spatial delayed alternation. *Journal of neurophysiology*, 108(12):3276–3288.

Ito, H. T., Zhang, S.-J., Witter, M. P., Moser, E. I., and Moser, M.-B. (2015). A prefrontal–thalamo–hippocampal circuit for goal-directed spatial navigation. *Nature*, 522(7554):50.

Jones, M. W. and Wilson, M. A. (2005). Theta rhythms coordinate hippocampal-prefrontal interactions in a spatial memory task. *PLoS Biol*, 3(12):e402.

Jung, M. W., Qin, Y., McNaughton, B. L., and Barnes, C. A. (1998). Firing characteristics of deep layer neurons in prefrontal cortex in rats performing spatial working memory tasks. *Cereb Cortex*, 8(5):437–450.

Karlsson, M. P., Tervo, D. G., and Karpova, A. Y. (2012). Network resets in medial prefrontal cortex mark the onset of behavioral uncertainty. *Science*, 338(6103):135–139.

Laskowski, C. S., Williams, R. J., Martens, K. M., Gruber, A. J., Fisher, K. G., and Euston, D. R. (2016). The role of the medial prefrontal cortex in updating reward value and avoiding perseveration. *Behavioural Brain Research*, 306:52–63.

Laubach, M., Amarante, L. M., Swanson, K., and White, S. R. (2018). What, if anything, is rodent prefrontal cortex? *eNeuro*, 5.

Laubach, M., Caetano, M. S., and Narayanan, N. S. (2015). Mistakes were made: neural mechanisms for the adaptive control of action initiation by the medial prefrontal cortex. *Journal of Physiology-Paris*, 109(1):104–117.

Libby, A. and Buschman, T. J. (2019). Rotational dynamics reduce interference between sensory and memory representations. *bioRxiv*, page 641159.

Lundqvist, M., Herman, P., and Miller, E. K. (2018). Working memory: Delay activity, yes! persistent activity? maybe not. *Journal of neuroscience*, 38:7013–7019.

Maggi, S., Peyrache, A., and Humphries, M. D. (2018). An ensemble code in medial prefrontal cortex links prior events to outcomes during learning. *Nature Communications*, 9.

Maingret, N., Girardeau, G., Todorova, R., Goutierre, M., and Zugaro, M. (2016). Hippocampo-cortical coupling mediates memory consolidation during sleep. *Nature Neuroscience*, 19:959–964.

Miller, P., Brody, C. D., Romo, R., and Wang, X.-J. (2005). A recurrent network model of somatosensory parametric working memory in the prefrontal cortex. *Cereb Cortex*, 15:679–679.

Murray, J. D., Bernacchia, A., Roy, N. A., Constantinidis, C., Romo, R., and Wang, X.-J. (2017). Stable population coding for working memory coexists with heterogeneous neural dynamics in prefrontal cortex. *Proceedings of the National Academy of Sciences of the United States of America*, 114:394–399.

Narayanan, N. S. and Laubach, M. (2008). Neuronal correlates of post-error slowing in the rat dorsomedial prefrontal cortex. *J Neurophysiol*, 100:520–525.

572 Peyrache, A., Khamassi, M., Benchenane, K., Wiener, S. I., and Battaglia, F. P. (2009).
573 Replay of rule-learning related neural patterns in the prefrontal cortex during sleep.
574 *Nature Neuroscience*, 12:919–926.

575 Poucet, B., Lucchessi, H., and Thinus-Blanc, C. (1991). What information is used by rats
576 to update choices in the radial-arm maze? *Behav Processes*, 25:15–26.

577 Powell, N. J. and Redish, A. D. (2016). Representational changes of latent strategies in
578 rat medial prefrontal cortex precede changes in behaviour. *Nature Communications*, 7.

579 Rich, E. L. and Shapiro, M. (2009). Rat prefrontal cortical neurons selectively code
580 strategy switches. *Journal of Neuroscience*, 29(22):7208–7219.

581 Rich, E. L. and Shapiro, M. L. (2007). Prelimbic/infralimbic inactivation impairs mem-
582 ory for multiple task switches, but not flexible selection of familiar tasks. *J Neurosci*,
583 27(17):4747–4755.

584 Rigotti, M., Barak, O., Warden, M. R., Wang, X.-J., Daw, N. D., Miller, E. K., and Fusi,
585 S. (2013). The importance of mixed selectivity in complex cognitive tasks. *Nature*,
586 497(7451):585–590.

587 Russo, E., Ma, T., Spanagel, R., Durstewitz, D., Toutounji, H., and Köhr, G. (2020).
588 Coordinated prefrontal state transition leads extinction of reward-seeking behaviors.
589 *bioRxiv*.

590 Sawangjit, A., Oyanedel, C. N., Niethard, N., Salazar, C., Born, J., and Inostroza, M.
591 (2018). The hippocampus is crucial for forming non-hippocampal long-term memory
592 during sleep. *Nature*, 564(7734):109.

593 Siegel, M., Buschman, T. J., and Miller, E. K. (2015). Cortical information flow during
594 flexible sensorimotor decisions. *Science*, 348(6241):1352–1355.

595 Singh, A., Peyrache, A., and Humphries, M. D. (2019). Medial prefrontal cortex population
596 activity is plastic irrespective of learning. *Journal of Neuroscience*, pages 1370–17.

597 Spaak, E., Watanabe, K., Funahashi, S., and Stokes, M. G. (2017). Stable and dynamic
598 coding for working memory in primate prefrontal cortex. *The Journal of neuroscience*
599 *: the official journal of the Society for Neuroscience*, 37:6503–6516.

600 Spellman, T., Rigotti, M., Ahmari, S. E., Fusi, S., Gogos, J. A., and Gordon, J. A. (2015).
601 Hippocampal-prefrontal input supports spatial encoding in working memory. *Nature*,
602 522(7556):309–314.

603 Stickgold, R. (2005). Sleep-dependent memory consolidation. *Nature*, 437(7063):1272.

604 Sul, J. H., Kim, H., Huh, N., Lee, D., and Jung, M. W. (2010). Distinct roles of rodent
605 orbitofrontal and medial prefrontal cortex in decision making. *Neuron*, 66(3):449–460.

606 Tononi, G. and Cirelli, C. (2014). Sleep and the price of plasticity: from synaptic and
607 cellular homeostasis to memory consolidation and integration. *Neuron*, 81(1):12–34.

608 Wasmuht, D. F., Spaak, E., Buschman, T. J., Miller, E. K., and Stokes, M. G. (2018).
609 Intrinsic neuronal dynamics predict distinct functional roles during working memory.
610 *Nature communications*, 9:3499.

Wimmer, K., Nykamp, D. Q., Constantinidis, C., and Compte, A. (2014). Bump attractor dynamics in prefrontal cortex explains behavioral precision in spatial working memory. *Nature Neuroscience*, 17:431–439.

Young, J. J. and Shapiro, M. L. (2009). Double dissociation and hierarchical organization of strategy switches and reversals in the rat pfc. *Behavioral Neuroscience*, 123:1028–1035.

Methods

Task description and electrophysiological data

All the data in this study comes from previously published data (Peyrache et al., 2009). The full details of training, spike-sorting and histology can be found in (Peyrache et al., 2009). The experiments were carried out in accordance with institutional (CNRS Comité Opérationnel pour l'Ethique dans les Sciences de la Vie) and international (US National Institute of Health guidelines) standards and legal regulations (Certificate no. 7186, French Ministère de l'Agriculture et de la Pêche) regarding the use and care of animals.

Four Long-Evans male rats were implanted with tetrodes in the medial wall of prefrontal cortex, covering the prelimbic and infralimbic regions, and trained on a Y-maze task (Figure 1a). During each session, neural activity was recorded for 20-30 minutes of sleep or rest epoch before the training phase, in which rats worked at the task for 20-40 minutes. After that, another 20-30 minutes of sleep or rest epoch recording followed. During the sleep epochs, intervals of slow-wave sleep were identified offline from the local field potential (details in Peyrache et al., 2009; Benchenane et al., 2010).

The Y-maze had symmetrical arms, 85 cm long, 8 cm wide, and separated by 120 degrees, connected to a central circular platform (denoted as the choice point throughout). Each rat worked at the task phase by self-initiating the trial, leaving the beginning of the start arm. A trial finished when the rat reached the end of the chosen goal arm. If the chosen arm was correct according to the current rule, the rat was rewarded with drops of flavoured milk. As soon as the animal reached the end of the chosen arm an inter-trial interval started and lasted until the rat completed its self-paced return to the beginning of the start arm.

Each rat was exposed to the task completely naïve and had to learn the rule by trial-and-error. The rules were presented in sequence: go to the right arm; go to the cued arm; go to the left arm; go to the uncued arm. The light cues at the end of the two arms were lit in a pseudo-random sequence across trials, regardless of the rule in place.

The recording sessions taken from the study of Peyrache and colleagues (Peyrache et al., 2009) were 53 in total. Each of the four rats learnt at least two rules, and they respectively contributed 14, 14, 11, and 14 sessions. The learning, rule change, and other sessions for each rat were intermingled. We used 49 sessions for most of the analysis. One session was omitted for missing position data, one for consistent choice of the right arm (in a dark arm rule) preventing decoder analyses (see below), and one for missing spike data in a few trials. An additional session was excluded for having only two neurons firing in all trials. Tetrode recordings were spike-sorted within each recording session. In the sessions we analysed here, the populations ranged in size from 4-25 units. Spikes were recorded with a resolution of 0.1 ms. Simultaneous tracking of the rat's position was recorded at 30 Hz.

Behavioural analysis

Each session was classified according to its behavioural features. The learning sessions were identified according to the original study (Peyrache et al., 2009) as the ones with three consecutive correct trials followed by a performance of at least 80% correct. The first of the three correct trials was the learning trial. Only ten sessions satisfied this criterion. We quantified this learning as a step-like change in performance by fitting a robust regression line to the cumulative reward curve before and after the learning trial. The slopes of the two lines gave us the rate of reward accumulation before (r_{before}) and after (r_{after}) the learning trial.

Eight rule change sessions were characterised by 10 consecutive correct trials or eleven correct out of twelve trials followed by a change in the rule. The first trial with the new rule was identified as the rule change trial. The change in performance in these sessions was quantified with the same method above, with a robust regression line was fitted to the cumulative reward curve before and after the rule change trial.

For all remaining sessions that were not rule change or putative learning sessions, we assessed any performance change by fitting the piece-wise linear regression model to each trial in turn (allowing a minimum of 5 trials before and after each tested trial). We then found the trial at which the increase in slope ($r_{after} - r_{before}$) was maximised, indicating the point of steepest inflection in the cumulative reward curve. We found 22 further sessions, labelled "minor-learning", in which we could find a positive inflection in the cumulative reward curve.

Linear decoding of task features

To predict which task feature was encoded in mPfC population activity we trained and tested a range of linear decoders (Hastie et al., 2009; Maggi et al., 2018). In the main text we report the results obtained using a logistic regression classifier, but for robustness we also tested three other decoders – linear discriminant analysis, (linear) support vector machines, and a nearest neighbours classifier – and found similar results. The full details of the decoding analysis can be found in Maggi et al. (2018).

Briefly, for each session, using the N active neurons in that session we constructed a N-length vector of their firing rates in each trial $\mathbf{r}$, resulting in the set of population firing rate vectors $\{\mathbf{r}(1), \ldots, \mathbf{r}(T)\}$ across the T trials. Each trial's task information was binary labelled for three features: outcome (labels: 0, 1), the chosen arm (labels: left, right) and the position of the light cue (labels: left, right). We used leave-one-out cross-validation to decode each feature, holding out the ith trial's vector $\mathbf{r}(i)$, training the classifier on the $N-1$ remaining trial vectors, and then using the resulting weight vector to predict the feature's label for the held-out trial. We quantified the accuracy of the decoder as the proportion of correctly predicted labels over all T held out trials. The same approach was used for the inter-trial intervals, by constructing $\mathbf{r}$ for the firing rates in each inter-trial interval.

For decoding at different positions in the maze, we first linearised the maze in five equally-sized sections then computed the firing rate vector of the core population of length N for each position p, $\mathbf{r^p}$. For each trial $t = 1, \ldots, T$ and each section of the maze $p = 1, \ldots, 5$, the set of population firing rate vectors $\{\mathbf{r^p}(1), \ldots, \mathbf{r^p}(T)\}$ was used to train the decoder.

For each rat and each session, the distribution of outcomes and arm choices depended on the rats' performance, which could differ from 50%. Therefore, we trained and cross-validated the same classifier on the same data-sets, but shuffling the labels of the task

features. In this way we obtained the accuracy of detecting the right labels by chance. We repeated the shuffling and fitting 50 times and we averaged the accuracy across the 50 repetitions.

Testing for independent encoding

To compare the decoding accuracy between trials and inter-trial intervals, we trained again the classifier using the population firing rate vectors computed on the entire maze $\{\mathbf{r}(1), \ldots, \mathbf{r}(T)\}$. We then trained the classifier on all the trials. We saved the population vector of weights and we tested the model, optimised to decode trial activity, on every inter-trial interval to evaluate the accuracy in decoding retrospective inter-trial interval labels. The same procedure was used to train the linear classifier on all the inter-trial intervals to test its accuracy in decoding trials activity. The population vector of weight was also saved for this model.

The angle, θ, between the population vector of trials', w_t, and inter-trial intervals', w_I, weights was computed as $\theta = \cos^{-1}\left(\frac{w_t \cdot w_I}{\|w_t\|\|w_I\|}\right)$.

We further evaluated the independence of trial and inter-trial interval population vectors by quantifying their separability in a low dimensional space. We used principal components analysis (PCA) to project the population vectors of a session onto a common set of dimensions. To do so, we constructed the data matrix $\mathbf{X}$ from the firing rate vectors of the core population, by concatenating trials and inter-trial intervals in their temporal order $\{\mathbf{r}_t(1), \mathbf{r}_I(1), \ldots, \mathbf{r}_t(T), \mathbf{r}_I(T)\}^{\mathrm{T}}$; the resulting matrix thus had dimensions of $2T$ rows and N (neurons) columns. Applying PCA to $\mathbf{X}$, we projected the firing rate vectors on to the top d principal axes (eigenvectors of $\mathbf{X^T X}$) to create the top d principal components. For each set of d components, we quantified the separation between the projected trial and inter-trial interval population vectors using a linear classifier (Support Vector Machine, SVM), and report the proportion of misclassified vectors. We repeated this for between $d = 1$ and $d = 4$ axes for each session.

Reactivation of task-feature encoding in sleep

In order to quantify the reactivation of waking activity in pre- and post-session sleep, we used the population firing rate vectors computed for the decoder $\{\mathbf{r}(1), \ldots, \mathbf{r}(T)\}$. We considered here the average population vector for each session, computed across all the trials for each feature. For example, we quantified the average population firing rate vector for all the right choice trials, and separately for all the left choice trials. We then compare the ranked average population firing rate vector for each feature with the firing rate vector of each 1 second time bin of slow-wave sleep pre- and post-session. We used Spearman's correlation coefficient to compare them and to quantify the difference between the distributions of each feature and the slow-wave sleep pre- and post-session. Spearman's coefficient was chosen specifically to remove any effects of global rate variations across the vectors within or between epochs.

In order to have a reactivation of activity in post-session sleep, we expected the distribution of Spearman correlation coefficient between a feature and pre-session slow-wave sleep to be leftward shifted compare to the distribution of Spearman correlation coefficient between the same feature and post-session slow-wave sleep. We quantified this shift by measuring the difference in the medians ($M_{post} - M_{pre}$) between the two distributions of correlation coefficients. If the difference was positive then we had a higher correlation of the population firing vector with the post-session slow-wave sleep compared to the pre-session slow-wave sleep. If negative, then the population firing rate vector was more

similar to the pre-session slow-wave sleep population vector. To then control for different time scales of reactivation in sleep we repeated the same procedure changing the time bin in the slow-wave sleep pre- and post-session. We used time bins from 100 ms to 10 sec every 150 ms for trials and from 10 sec to 200 sec every 2 sec for inter-trial intervals.

Data Availability

The spike-train and behavioural data that support the findings of this study are available in CRCNS.org (DOI: 10.6080/K0KH0KH5), originating from (Peyrache et al., 2009). Code to reproduce the main results of the paper is available at: [URL to come]